Earthquakes and Structures, *Vol. 4, No. 5 (2013) 527-555*
DOI: http://dx.doi.org/10.12989/eas.2013.4.5.527

Probabilistic seismic demand models and fragility estimates for reinforced concrete bridges with base isolation

Paolo Gardoni*[1] and David Trejo[2]

[1]*Department of Civil and Environmental Engineering, University of Illinois at Urbana-Champaign, Urbana, IL 61801, USA*
[2]*School of Civil and Construction Engineering, Oregon State University, Corvallis, OR 97331, USA*

(Received March 31, 2011, Revised November 10, 2011, Accepted January 3, 2013)

Abstract. This paper proposes probabilistic models for estimating the seismic demands on reinforced concrete (RC) bridges with base isolation. The models consider the shear and deformation demands on the bridge columns and the deformation demand on the isolation devices. An experimental design is used to generate a population of bridges based on the AASHTO LRFD Bridge Design Specifications (AASHTO 2007) and the Caltrans' Seismic Design Criteria (Caltrans 1999). Ground motion records are used for time history analysis of each bridge to develop probabilistic models that are practical and are able to account for the uncertainties and biases in the current, common deterministic model. As application of the developed probabilistic models, a simple method is provided to determine the fragility of bridges. This work facilitates the reliability-based design for this type of bridges and contributes to the transition from limit state design to performance-based design.

Keywords: seismic demand; probabilistic model; experimental design; finite element; highway bridge; base isolation; seismic fragility; importance analysis

1. Introduction

Bridges are key links in the transportation system, and they have shown significant vulnerability to earthquakes. Most recently, damage to 174 major bridges, including cracks or failures of the bridge piers, caused traffic interruption after the 2008 Wenchuan Earthquake (Qiang *et al.* 2009). Isolation bearings can isolate the heavy bridge superstructure from the substructures, such as the abutments and piers, avoiding or reducing damage to the structures. Thus, it is important to understand and form proper models to predict the performance of bridges with isolation bearings.

Many studies have been performed to investigate the performance of bridges with base isolation and to develop design procedures for new and retrofitted bridges (Priestley *et al.* 1996, Kelly and Naeim 1999, Wilde *et al.* 2000). Karim and Yamazaki (2003, 2007) developed seismic fragility models for base-isolated bridges. However, as recognized by Karim and Yamazaki (2003, 2007), the fragility models developed are not transportable to other bridges because modeling and estimation is carried out at the structural system level. That is, the fragility estimate for a specific

*Corresponding author, Professor, E-mail: gardoni@illinois.edu

http://www.techno-press.org/?journal=eas&subpage=7 ISSN: 2092-7614 (Print), 2092-7622 (Online)

structural system cannot be used to assess the fragility of another structure, except as a crude approximation. In addition, ideally the fragility models should be derived from first principles, e.g. the rules of mechanics. However, assuming an arbitrary distribution function (e.g. lognormal) to express the fragility curve and estimating its distribution parameters have no direct physical interpretation.

This paper puts forward a state-of-the-art approach to assess such reliability accounting for available information, including mechanical models and engineering knowledge. The proposed approach can be used to quantify the actual benefits of constructing or retrofitting a bridge with base-isolation in terms of improved reliability. Such information is needed for the best allocation of available resources. The proposed formulation maintains the simplicity required for its implementation in practice and therefore has the potential to have a real impact on the implementation of reliability-based design.

In this study, we develop probabilistic models to determine seismic demands on single-column bent RC bridges using laminated rubber isolators and provide a simple formulation to estimate the seismic fragility of these structures. The methodology presented in this paper can be used to develop probabilistic models for other types of isolated bridges with only different considerations on the design parameters. To facilitate their acceptance, the proposed probabilistic models are constructed by developing correction terms to simplified analysis procedures commonly used in practice. To provide data for the model development, time-history analyses on 60 typical bridges are carried out. The sample bridges are designed according to Caltrans (1999) and AASHTO (2007). To provide a representative and diverse sample of bridges, combinations of the basic design parameters are obtained using an experimental design (Sacks *et al.* 1989). An experimental design is defined in this paper as a statistical process used to select the values of the considered parameters in order to maximize the amount of "information" that can be obtained for a given amount of experimental effort (e.g. number of experiments or simulations). The non-linear time-history analysis on each bridge provides structural response quantities, such as the shear and deformation of the bridge column and the deformation of the isolation device. The probabilistic demand models can be of value in providing unbiased estimates of the deformation and shear demands and can efficiently assess the reliability of reinforced concrete (RC) bridges for performance- and reliability-based design.

To develop the seismic reliability model, the capacity models developed by Kelly and Naeim (1999), Gardoni *et al.* (2002) and Choe *et al.* (2007) are used in combination with the proposed probabilistic demand models. Importance analysis is carried out to determine the random variables that have the main effects on the probability of failure of RC bridges using laminated rubber isolators. Based on the results of the importance analysis, a simple and accurate formulation is developed to estimate the seismic fragility of these structures. The proposed reliability formulation is used for a reliability-based optimal design of the base isolation system.

This paper is organized into eight sections including this introduction section. The following section presents the details on the bridge models and the dynamic analyses including the experimental design, the selection of the ground motions, and the results of the nonlinear time-history analysis. In the third section, we describe the development of the probabilistic demand models. We then present the capacity models used for the reliability analysis. The fifth section describes the formulation of the approximate fragility estimates. Next, we present the reliability-based optimal design of base isolation systems. We then present an application of the proposed models to the fragility of an example bridge and follow this with conclusions from the research.

2. Bridge models and dynamic analysis

This section describes the design parameters of the isolated RC bridges, the experimental design used to generate the sample bridges, and the selection of the ground motion records for the dynamic analysis of the finite element (FE) models of these bridges. A three-dimensional model for each sample bridge is developed using OpenSees (McKenna *et al.* 2003). Nonlinear time history analysis of each bridge is performed to produce structural responses needed to construct the probabilistic models.

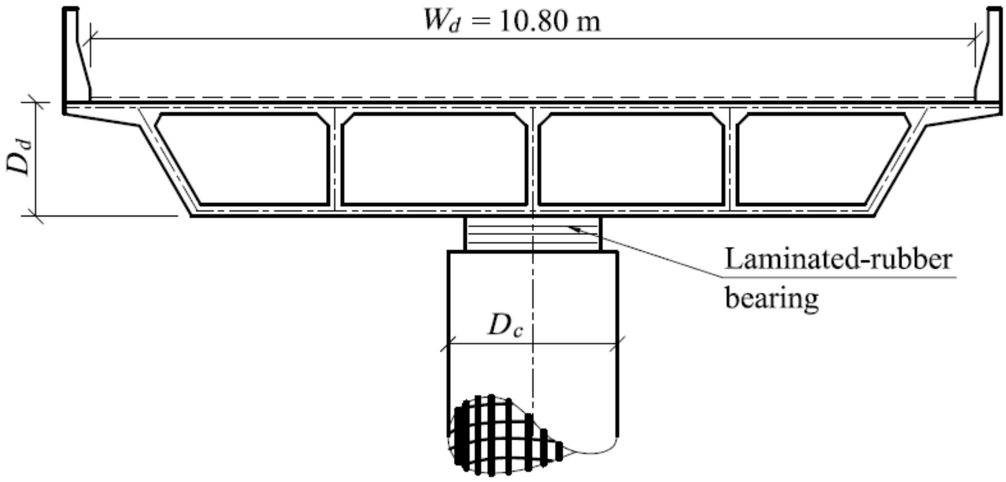

Fig. 1 Cross section of the superstructure of a typical base-isolated bridge with its pier

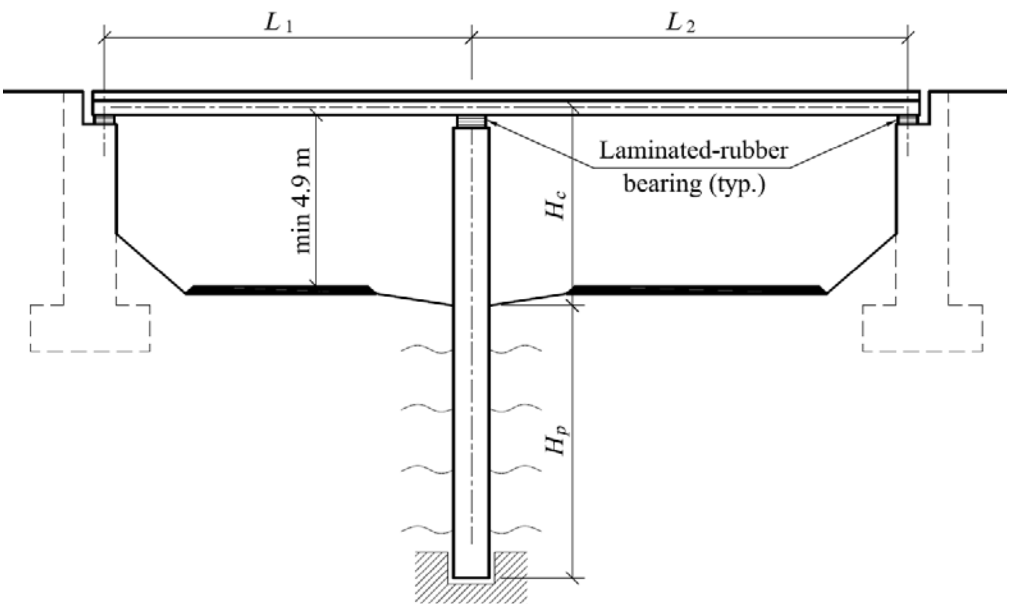

Fig. 2 Typical configuration of the base-isolated bridges

2.1 Description of bridges

Design parameters of a base-isolated bridge are selected based on AASHTO (2007) and Caltrans (1999). The superstructure is a cast-in-place RC multi-cell box girder with a monolithic concrete deck as defined in Section 4 of the AASHTO specifications. Each bridge has three design lanes with the clear roadway width, W_d, of 10.80 m as shown in Fig. 1. In the figure, D_c and D_d represent the column diameter and the deck depth, respectively. The span/depth ratio is 18 as is typical for non-prestressed box girders (Barker and Puckett 2007). As shown in Fig. 2, laminated-rubber or elastomeric bearings are located at the abutments and on the pier top to decouple the vibration of the superstructure and the substructures. It is assumed that two square bearings are designed to be placed between the deck and the abutment, and a circular bearing between the deck and the pier. Fig. 1 shows the arrangement at the pier while Fig. 2 shows the arrangement of the bearings for the bridge. Note that Fig. 2 only shows the typical configuration of

Table 1 Design parameters for base-isolated bridges with one single-column bent

Design parameter	Range	Number of strata
Degree of skew, α_{skew}	0^o – 60^o	61
Range of span length, L_2	15 – 39 m	50
Span ratio, L_2 / L_1	1 – 1.5	50
Column height, H_c	5 – 11 m	20
Column-diameter-to-deck-depth ratio, D_c / D_d	0.67 – 1.33	20
Reinforcement nominal yield strength, f_y	414 – 517 MPa	20
Concrete compressive strength, f_c'	28 – 55 MPa	20
Longitudinal reinforcement ratio of the column, ρ_l	1 – 4%	30
Transverse reinforcement ratio of the column, ρ_t	0.4 – 1.1%	30
Additional superstructure weight, w_{as}	10 – 75%	60
Soil types, USGS Classification, K_{soil}	A, B, C and D	4
Number of inner elastomer layers of a bearing, n_e	3 – 15	13
Thickness of each inner elastomer layer, t_e	7.6 – 38 mm	12
Shape factor of the thickest elastomer layer, S_b	3 – 40	60
Shear modulus of elastomer, G_b	552 – 1207 Pa	60
Pile depth/column height ratio, H_p / H_c	1 – 3	20
Abutment backwall stiffness, K_l	10 – 30 kN/mm/m	30
Abutment transverse stiffness, K_t	105 – 210 kN/mm	60

this class of bridges. Fig. 2 also provides the definitions of other model parameters, such as the pile depth, H_p, the column height, H_c, and bridge spans, L_1 and L_2.

The design parameters that completely define each base-isolated bridge are divided into “basic” and “derived” parameters. Table 1 provides the ranges of the basic parameters considered in the experimental design in which each range is divided into a number of strata. The additional dead load, w_{as}, due to the railing systems, the transverse diaphragm, the wearing surface, and attachments participates in the vibration and affects the response of the entire structural system. This load is assumed to vary from 10 to 75 percent of the weight of the structural deck, similar to the assumption by Mackie and Stojadinovic (2003). A soil is classified following the USGS Site Classifications as A, B, C, or D (PEER 2009), with corresponding average shear wave velocities (to a depth of 30 m) greater than 750 m/s, 360-750 m/s, 180-360 m/s and less than 180 m/s, respectively. The remaining derived variables are obtained by designing each bridge according to AASHTO LRFD Bridge Design Specifications (AASHTO 2007) and Caltrans’ Seismic Design Criteria (Caltrans 1999).

2.2 Experimental design for bridge models

A population of isolated bridges is formed by conducting an experimental design using the Space-Filling Design technique in which the Stratified Latin Hypercube sampling is used to ensure that each design parameter has all portions of its domain represented (Sacks *et al.* 1989). The Space-Filling experimental design is used to fill up the space of the design parameters in a uniform fashion (Bates *et al.* 1996).The range of each design parameter is partitioned into strata and a representative value is selected from each stratum. Each bridge is formed by combining the representative values of each design parameter such that every representative value is used at least once in the whole process. The combination of representative values is oriented so that the distance between one selected point that corresponds to one bridge and the other points is maximized. As a result, 60 isolated RC bridges are obtained. The period of this bridge population that is computed based on the elastic stiffness of the pushover curve varies from 0.274 to 3.174 seconds (Table 2).

2.3 Selection of ground motion records

Representative ground motion records are selected for the nonlinear time-history dynamic analyses of the sample bridges following the bin method in Shome and Cornell (1999) and Huang

Table 2 Range of quantities of interest for the base-isolated bridges

Quantity	Range
Natural period, T_1	0.274 – 3.174 s
Elastic stiffness of the isolation bearings, K_i	0.468 – 423.767 MN/m
Post-yield stiffness of the isolation bearing, K_h	0.151 – 55.785 MN/m
Characteristic strength of the isolation bearing, Q	0.542 – 422.260 MN

et al. (2010). In particular, Huang *et al.* (2010) developed probabilistic demand models for RC bridges without base isolation. To assess the effects of based isolation on the performance and reliability of bridges, the same ground motions are used in this study. Following Shome and Cornell (1999), the selected ground motions are subdivided into five bins based on moment magnitude (M) and the closest distance between the record location and the rupture zone (R). Each bin represents specific combinations of the earthquake characteristics and the collection of all bins captures all possible characteristics. Thus, each bin should have (1) enough earthquakes to capture the variability of the characteristics of that bin and (2) the same number of ground motions as each of the other bins.

Five bins are defined based on M and R. Following Huang *et al.* (2010), the five bins used are:
(1) SMSR – Small Magnitude, Short Range: M = [5.5, 6.5]; R = [15 km, 30 km]
(2) SMLR – Small Magnitude, Long Range: M = [5.5, 6.5]; R = [30 km, 50 km]
(3) LMSR – Large Magnitude, Short Range: M = [6.5, 7.5]; R = [15 km, 30 km]
(4) LMLR – Large Magnitude, Long Range: M = [6.5, 7.5]; R = [30 km, 50 km]
(5) NEAR – Near Field: M = [6.0,7.5]; R = [0 km, 15 km]

Following the classification in Abrahamson and Silva (1997), to account for the effects of soil amplification due to different soil characteristics, the ground motions are divided into two groups. Group 1 contains the motions recorded from Site Classes A and B, “rock and shallow” sites, and Group 2 contains those from other site classes, “deep soil” sites. Each group has the five bins listed earlier, which gives a total of 10 bins. For each bin 20 earthquakes are selected from the Pacific Earthquake Engineering Research (PEER) Center Strong Motion Catalog (PEER 2009) so that the median pseudo-spectral acceleration (PSA) value for each bin is close to the corresponding theoretical value obtained using the attenuation law in Abrahamson and Silva (1997).

Following Luco (2002), to study the responses of bridges due to larger earthquakes, Huang *et al.* (2010) generated additional ground motions by multiplying the earthquake acceleration records in each bin by 8 for the ground motions in Bins I-IV and by 2 for the near-field ground motions (Bin V). This scaling process created 10 additional bins (5 for each soil type).

In addition to the ground motions in Huang *et al.* (2010), 34 ground motions with the highest

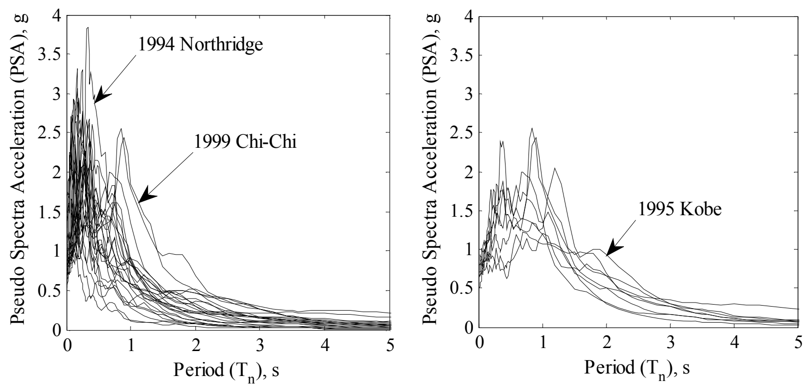

(a) (b)

Fig. 3 Pseudo spectra acceleration of additionally selected strong ground motions values of PSA from all available records in the PEER Catalog are also selected for this analysis to supplement the data points in the upper tail of the structural dynamic responses and to better investigate the nonlinear behavior of the bridge columns. Fig. 3 shows the PSA of the 34 records with the highest PSA including those from the well-known Northridge, Chi-Chi and Kobe Earthquakes (which will be used in a later section to show a comparison between the fragility of an isolated and a non-isolated example bridge). The ground motion associated to the 1994 Northridge Earthquake was recorded at the Tarzana – Cedar Hill AStation (SN #341, where SN is the unique sequence number of the station). The ground motion associated to the 1995 Kobe Earthquake was recorded at the Takatori Station (SN #940). The ground motion associated to the 1999 Chi-Chi Earthquake was recorded at the CHY080 Station (SN #681). This set of selected records includes all the ground motions with PSA values greater than 2.0 g for periods less than 1.0 s and all those with PSA values greater than 1.0 g for the greater periods. The accelerograms of these ground motions are also scaled up by the factor of 2.0 and 4.0 respectively for the former and the latter. While there is a degree of arbitrariness in the scaling factors, the addition of the scaled ground motions is intended to supplement the data in the upper tail of the structural dynamic responses and allow for a better investigation of the nonlinear behavior of the bridge columns.

For each of the 60 base-isolated bridges, 12 ground motions are randomly selected, one from each bin (5 not scaled and 5 scaled) and one from each two additional suites of ground motions with high values of PSA (1 not scaled and 1 scaled). Sampling without replacement is used for the random selection to ensure that all ground motions are used for the analyses. All earthquake records are applied in three orthogonal directions, where one of the two horizontal components is randomly assigned to the bridge transverse direction and the other horizontal component to the bridge longitudinal direction.

2.4 FE models and nonlinear time history analysis

Under seismic load, the bridge deck is expected to remain elastic (Priestley *et al.* 1996), therefore, it is modeled using elastic elements. Nonlinear fiber elements are used to model the

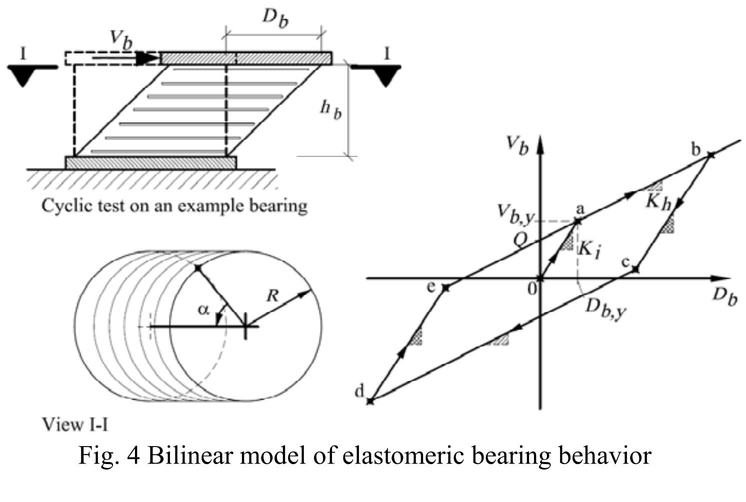

Fig. 4 Bilinear model of elastomeric bearing behavior

Table 3 Design parameters of the example bridge

Parameter	Distribution	Value/Mean	Standard deviation
Abutment skew, α_{skew} (°)	-	0.000	-
Right span, L_2 (m)	Lognormal	38.100	0.381
Span ratio, L_2 / L_1	-	1.250	-
Column height, H_c (m)	Lognormal	6.706	0.067
Column diameter, D_c (m)	Lognormal	1.572	0.031
Pile-to-column length ratio, H_p / H_c	-	1.500	-
Concrete cover, c_{conc} (m)	Lognormal	0.038	0.004
Longitudinal steel yield strength, f_y (MPa)	Lognormal	437.835	21.892
Transverse steel yield strength, f_{yh} (MPa)	Lognormal	350.268	17.513
Concrete compressive strength, f_c' (MPa)	Lognormal	35.027	3.503
Longitudinal reinforcement ratio, ρ_l (%)	-	3.590	-
Transverse reinforcement ratio, ρ_t (%)	-	1.060	-
Longitudinal abutment stiffness, K_l (MPa)	Lognormal	20.000	4.000
Transverse abutment stiffness, K_t (MN/m)	Lognormal	110.000	22.000
Additional superstructure weight†, w_{as} (%)	Normal	45.000	11.250
Shape factor of the abutment bearing‡, S_{ba}	-	6.000	-
Shape factor of the column bearing‡, S_{bp}	-	12.000	-
Number of internal elastomer layers‡, n_e	-	9	-
Elastomer layer thickness‡, t_e(m)	Lognormal	0.020	0.002
Elastomer shear modulus‡, G_b (MPa)	Lognormal	0.900	0.180

†The uncertainty in the mass is taken into account by considering the uncertainty of the additional weight.
‡Properties only used for the based isolated example bridge

column and the drilled shaft. Rigid link elements and zero-length elements are used to model the abutment stiffness and the behavior of the elastomeric bearings. The interaction between the abutment and the deck end is modeled with elements using a compression gap material (McKenna *et al.* 2003). The elements behave in the way that the stiffness of the abutment will limit the horizontal displacement of the deck if the deck end displaces toward the abutment back wall. To reflect the variability in the soil type, four different stiffnesses are considered based on the USGS (U.S. Geological survey) soil classification. The properties for each spring type can be found in Mackie and Stojadinović (2003). The hysteretic response of the bearings under lateral loading has significant effects on the behavior of a base-isolated bridge system. The relation between the shear force, V_b, and the lateral deformation, D_b, of a bearing can be idealized as a bilinear model. This model is defined by three parameters: the elastic stiffness, K_i, the post-yield stiffness, K_h, and the characteristic strength, Q, as shown in Fig. 4. Table 2 presents the ranges of these three parameters that are computed from the experimental design using the bilinear model in Cheng *et al.* (2008). In the model, $V_{b,y}$ and $D_{b,y}$ denote the yield shear force and the yield lateral deformation. In the figure, dimensions h_b and R represent the height and the radius of the bearing, and α is the angle between the direction of deformation and the intersection of the top and bottom faces of the bearing. Cheng *et al.* (2008) showed that a bilinear model provides satisfactory estimation of the bearing behavior for small displacements. However, further works is

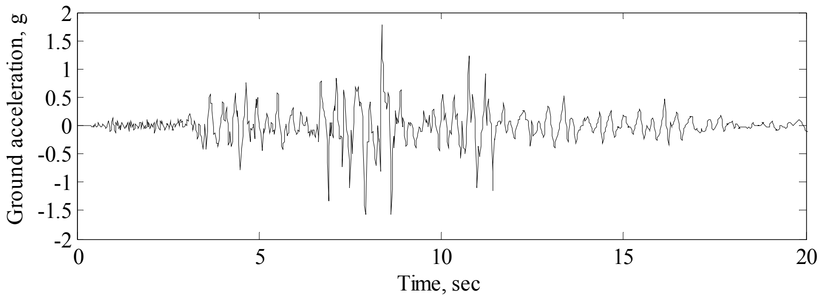

(a) Transverse ground acceleration

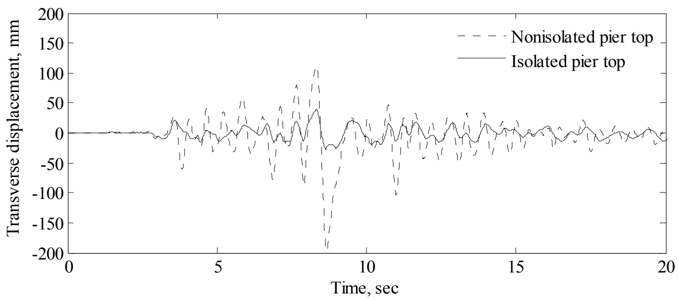

(b) Transverse displacement of pier top versus time

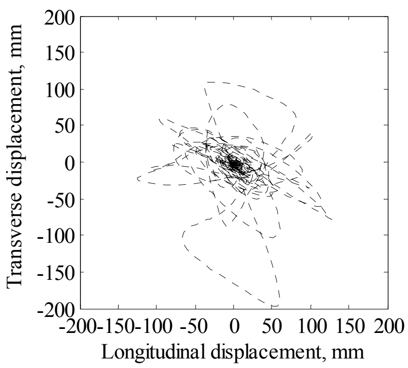

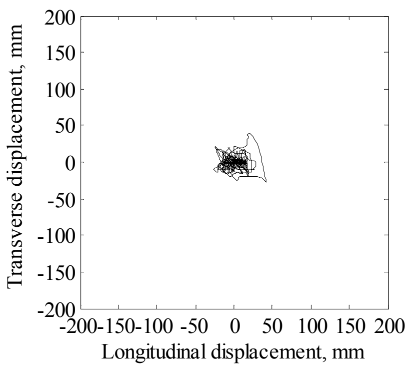

(c) Orbital displacement of the non-isolated pier top (d) Orbital displacement of the isolated pier top

Fig. 5 Performance of the example bridges under the 1994 Northridge Earthquake at the Tarzana Station necessary to develop a more accurate model for large displacements which is beyond the scope of this paper.

Fig. 5 shows the seismic behavior of an example isolated bridge and its corresponding non-isolated bridge under the ground motion associated to the Northridge Earthquake. The design parameters of the two bridges are the mean values in Table 3. The statistics of each design parameters in Table 3will be used for reliability analysis presented later in the paper. The non-isolated bridge is obtained by replacing the elastomeric bearing on the pier top with a fixed connection between the pier and the superstructure. It is assumed that the example bridges are built on a deep soil site (the USGS Classification C). The number of the inner elastomer layers, n_e, the elastomer layer thickness, t_e, and the elastomer shear modulus, G_b, are assumed to be the same for the bearings both at the abutments and at the pier. However, the two bearings at each abutment can support less vertical loads from the superstructure and hence they have a shape factor, S_{ba}, that is smaller than the shape factor, S_{bp}, for the bearing at the column. The period of the non-isolated bridge is 0.966 s, and that of the base-isolated bridge is 1.591 s. Fig. 5(a) shows the time history of the transverse ground acceleration. Fig. 5(b) shows the transverse displacement of the pier top of the isolated and non-isolated bridges. The peak displacement of the isolated pier top is less than 50 mm, which is approximately one-fourth of the peak displacement of the non-isolated bridge. Therefore, the seismic deformation demand on the pier is significantly reduced by using elastomeric bearings; the shear demand (not shown here for brevity) has a similar reduction. Figs. 5(c) and 6(d) show the orbital displacement of the pier top for the non-isolated and isolated bridges, respectively. The maximum horizontal displacements of the non-isolated bridge are more than 4 times the maximum horizontal displacements of the isolated bridge.

3. Probabilistic demand models

Following Gardoni *et al.* (2003), the proposed probabilistic demand models are developed from deterministic models and procedures that are commonly used in practice. Correction terms are developed to amend for the bias typically inherent in the deterministic models and procedures and to capture the underlying uncertainties. Probabilistic models are developed for the shear and deformation demands on RC columns and the deformation demand on the isolation bearings.

3.1 Modeling of structural demands

Following Gardoni *et al.* (2002, 2003), the demand quantity of interest D_k is modeled as

$$D_k\left(\mathbf{x},\mathbf{\Theta}_{D,k}\right)=\hat{d}_k\left(\mathbf{x}\right)+\gamma_{D,k}\left(\mathbf{x},\boldsymbol{\theta}_{D,k}\right)+\sigma_{D,k}\varepsilon_{D,k} \tag{1}$$

where D_k represents the column deformation $(k=\delta)$ and shear $(k=v)$, and the bearing deformation $(k=b)$ demands, $\hat{d}_k(\mathbf{x})$ is the demand quantity k predicted using a deterministic model (e.g. a code equation), $\gamma_{D,k}(\mathbf{x},\boldsymbol{\theta}_{D,k})$ is the correction term that captures the potential bias in $\hat{d}_k(\mathbf{x})$, $\sigma_{D,k}\varepsilon_{D,k}$ is the model error , where $\varepsilon_{D,k}$ is a random variable with zero mean and unit standard deviation, $\sigma_{D,k}$ represents the standard deviation of the model error, $\mathbf{x}$ is a vector of geometrical and material properties and ground motion characteristics, and $\mathbf{\Theta}_{D,k} = (\mathbf{\theta}_{D,k}, \sigma_{D,k})$ is a vector of unknown model parameters. Due to the non-negative nature of the demand quantities, in this formulation a natural logarithm transformation is used to approximately satisfy the following two assumptions: (1) $\sigma_{D,k}$ is not a function of $\mathbf{x}$ (homoskedasticity assumption) and (2) $\varepsilon_{D,k}$ has the standard normal distribution (normality assumption). In particular, we define $D_\delta = \ln(\Delta_c / H_c)$, $D_v = \ln[V_c / (f_t' A_c)]$, and $D_b = \ln(\Delta_b / h_b)$, where Δ_c is the column deformation demand, V_c is the column shear demand, Δ_b is the bearing deformation demand, f_t' is the tensile strength of concrete, and A_c is the cross-section area of the bridge column. The product of the concrete tensile strength and the column cross-sectional area is used herein to normalize the shear demand. In general, $\varepsilon_{D,\delta}$, $\varepsilon_{D,v}$, and $\varepsilon_{D,b}$ are correlated, with correlating coefficients $\rho_{D,\delta v}$, $\rho_{D,\delta b}$, and $\rho_{D,vb}$. Therefore the complete set of unknown parameters is $\mathbf{\Theta}_D = (\mathbf{\Theta}_{D,\delta}, \mathbf{\Theta}_{D,v}, \mathbf{\Theta}_{D,b}, \rho_{D,\delta v}, \rho_{D,\delta b}, \rho_{D,vb})$.

Different models and procedures can be used to formulate $\hat{d}_k(\mathbf{x})$. We use a modification of the Capacity-demand-diagram Method (Freeman 1998, Chopra and Goel 1999, Fajifar 1999) proposed by Gardoni *et al.* (2003), herein called modified capacity-demand-diagram method. The Modified Capacity-demand-diagram Method is based on the well-known capacity spectrum method, which has been adopted by the Applied Technology Council (ATC) and the Federal Emergency Management Agency (FEMA) in their documents ATC-40 (ATC 1996) and FEMA-274 (FEMA 1997). This approach is ideally suited because of its simplicity. Note that this selected deterministic demand model requires a pushover analysis, where the natural period is computed from the elastic stiffness of the pushover curve and half of the superstructure mass. Alternative approaches like the Modified Capacity Spectrum Method given in Procedure A of Report FEMA-440 (ATC 2005) could also be used but they would require iterative computation and convergence is not guaranteed. These limitations make the Modified Capacity Spectrum Method less practical.

The correction term $\gamma_{D,k}(\mathbf{x}, \mathbf{\theta}_{D,k})$ can be formulated as

$$\gamma_{D,k}\left(\mathbf{x}, \mathbf{\theta}_{D,k}\right) = \mathbf{\theta}_{D,k}^T \mathbf{H}_{D,k}\left(\mathbf{x}\right) \tag{2}$$

where $\mathbf{\theta}_{D,k}^T = [\theta_{D,k1}\ \theta_{D,k2}\ \cdots\ \theta_{D,kp_k}]$,and $\mathbf{H}_{D,k}^T(\mathbf{x}) = [h_{D,k1}(\mathbf{x})\ h_{D,k2}(\mathbf{x})\ \cdots\ h_{D,kp_k}(\mathbf{x})]$ is a vector of p_k explanatory variables. The unknown parameters, $\mathbf{\theta}_{D,k}$, are estimated along with $\sigma_{D,k}$ by calibrating the demand models in Eq. (1). The calibration is carried out using a Bayesian

Table 4 Candidate explanatory functions constituting the probabilistic models

Description	Normalized form, $h_{ki}(\mathbf{x})$
Constant	1
Deterministic demand estimate for quantity k	$\hat{d}_k(\mathbf{x})$
Elastic pseudo-spectral acceleration, PSA	$\ln(PSA/g)$
Pre-yield offset, $[d_k - d_{k,y}]_-$	$\begin{cases} d_k - d_{k,y}, \text{if } d_k \le d_{k,y} \\ 0, \text{if } a_k > d_{k,y} \end{cases}$
Post-yield offset, $[d_k - d_{k,y}]_+$	$\begin{cases} 0, \text{if } a_{k \le d_{k,y}} \\ d_k - d_{k,y}, \text{if } d_k > d_{k,y} \end{cases}$
Peak ground acceleration, PGA	$\ln(PGA/g)$
Peak ground velocity, PGV	$\ln(PGV \cdot T_1 / H_c)$
Peak ground displacement, PGD	$\ln(PGD / H_c)$
Earthquake attack angle, with respect to the longitudinal direction, θ_{EQ}	θ_{EQ} in degrees
Abutment skew, α_{skew}	α_{skew} in degrees
Pile-depth-to-column-height ratio, $r_{P/C}$	$\ln(H_P / H_C)$
Ratio of transverse to longitudinal stiffness of the abutment, r_A	$\ln[K_t / (K_l \cdot W_a)]$
Span ratio	$\ln(L_2 / L_1)$
Abutment bearing rotational stiffness, K_{ar}	$\ln[K_{ar} / (K_{ai} \cdot A_a)]$
Pier bearing rotational stiffness, K_{pr}	$\ln[K_{pr} / (K_{pi} \cdot A_p)]$
Soil classification	$K_{soil} = \begin{cases} 1 \text{ for soil types A \& B} \\ 0 \text{ for soil types C \& D} \end{cases}$
Number of inner elastomer layers[†], n_e	$\ln(n_{ea})$ and $\ln(n_{ep})$
Shape factor of the thickest elastomer layer[†], S_b	$\ln(S_{ba})$ and $\ln(S_{bp})$

[†] n_{ea}, S_{ba} for bearings the abutments; n_{ep}, S_{bp} for the bearing at the pier

approach (Box and Tiao 1992) with the demand data obtained from the FE analyses and, due to a lack of prior information, a non-informative prior.

Table 4 lists the candidate explanatory functions that are used to form the probabilistic demand models. To capture a potential constant bias in the deterministic model, we select the constant 1 as a candidate explanatory function. To detect any possible under- or over-estimation of the deterministic model, we also select $\hat{d}_k(\mathbf{x})$ and the elasticpseudo-spectral acceleration, PSA as potential explanatory functions. Different biases and uncertainties in the computation of the column deformation and shear using the deterministic model may depend on the elastic or inelastic behavior of the system. Thus, the explanatory functions $[d_k - d_{k,y}]$ and $[d_k - d_{k,y}]$ are included to represent the pre-yield and post-yield offsets, respectively, where $\hat{d}_{k,y}$ stands for the value of the response quantity k determined at yield using the deterministic model. The following quantities not accounted for in the deterministic demand model are also considered to construct candidate explanatory functions: the peak ground acceleration (PGA), the peak ground velocity (PGV), the peak ground displacement (PGD), the attack angle of the earthquake, θ_{EQ}, defined with respect to the longitudinal direction, the abutment skew angle, α_{skew}, the pile-depth-to-column-height ratio, $r_{P/C}$, the ratio of transverse to longitudinal stiffness of the abutment, r_A, the span ratio, L_2 / L_1, and soil types, K_{soil}. The characteristics and properties of the isolation bearings, such as the abutment and pier bearing rotational stiffnesses, K_{ar} and K_{pr}, the number of elastomer layers, n_e, and the shape factor of the elastomer layer, S_b, are also considered to construct candidate explanatory functions to account for the effects of the bearings on the seismic demands. As shown in Table 4, normalized forms are used to construct the candidate explanatory functions, where T_1 is the natural period of the structure, g is the gravity acceleration, W_a is the abutment width, K_{ai} and K_{pi} are the elastic stiffness values of the abutment and pier bearings, and A_a and A_p are the base areas of the abutment and pier bearings.

3.2 Model selection

To facilitate their use in practice, probabilistic models should be as parsimonious as possible. That is, based on the general formulation in Eq. (1), $\gamma_{D,k}(\mathbf{x}, \boldsymbol{\theta}_{D,k})$ should have as few explanatory functions are possible. For the three demand quantities of interest, Fig. 6 presents comparisons among alternative probabilistic demand models that have different numbers of explanatory functions. The three plots on the left side of Fig. 6 show the coefficient of determination R^2 (Weisberg 2005), the adjusted coefficient of determination R^2_{adj} (Sheather 2008), and the standard deviation of the model errors, $\sigma_{D,k}$, versus the number of explanatory functions. The higher the values of R^2 and R^2_{adj} are and the smaller the value of $\sigma_{D,k}$ is, the better the model is (however, caution should be exercised in the interpretation of R^2 since it does not account for the complexity of the model). Note that the coefficient of variation of the responses for quantity k can be computed through the variance of the model errors, $\sigma^2_{D,k}$, as $c.o.v._{D,k} = \sqrt{\exp(\sigma^2_{D,k}) - 1}$.

The right side of Fig. 6 presents the Akaike's information criterion (AIC) and the Bayesian information criterion (BIC) and are plotted again versus the number of explanatory functions. The smaller the values of AIC and BIC are, the better the model is. The models with the minimum

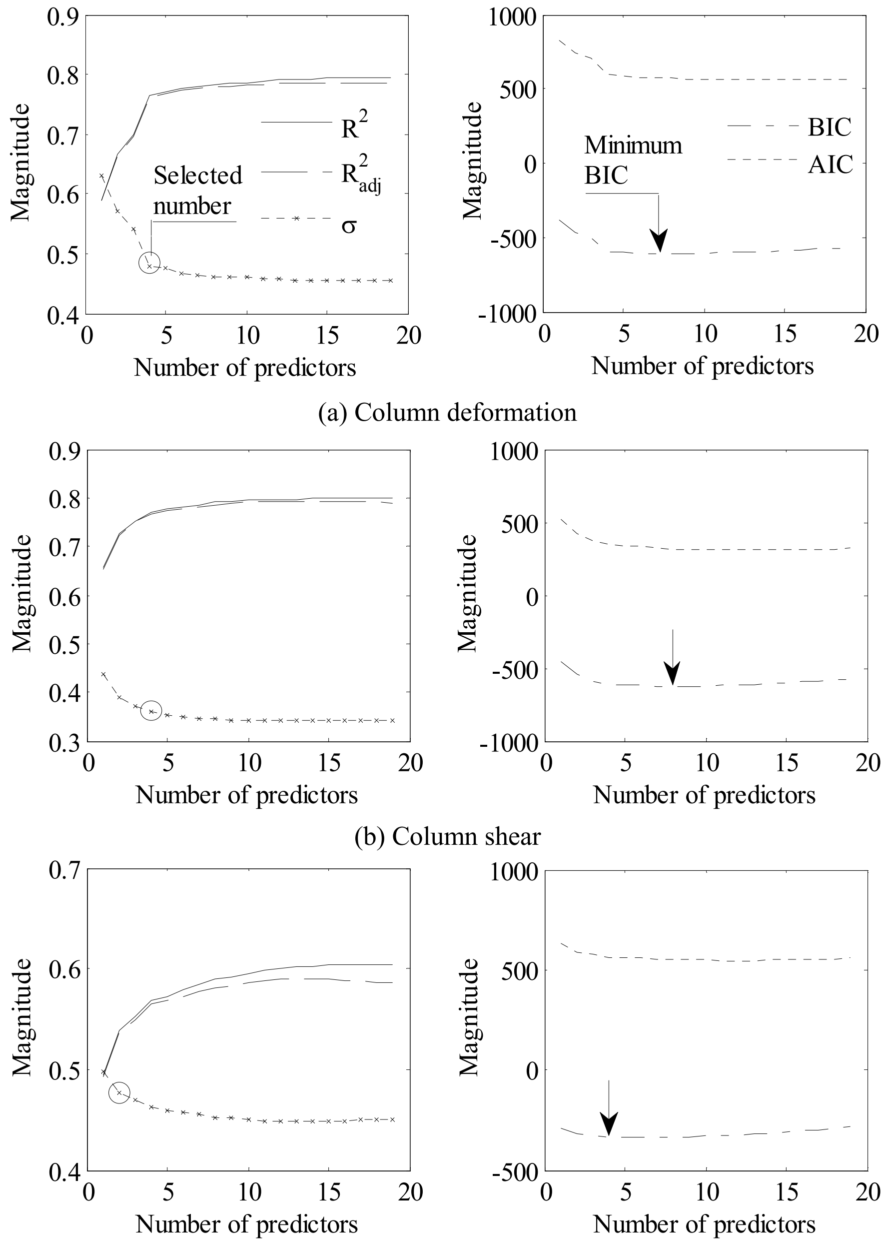

(a) Column deformation

(b) Column shear

(c) Bearing deformation

Fig. 6 Comparison of probabilistic models with different number of best explanatory functions

BIC values are identified in Fig. 6 with an arrow. Considering these five criteria, we select the following three correction terms marked with a circle in Fig. 6

$$\gamma_{D,\delta}\left(\mathbf{x},\boldsymbol{\theta}_{D,\delta}\right)=\theta_{D,\delta 1}\ln\left(\frac{PGA}{g}\right)+\theta_{D,\delta 2}\ln\left(\frac{K_{ar}}{K_{ai}\cdot A_{a}}\right)+\theta_{D,\delta 3}\ln\left(S_{ba}\right)+\theta_{D,\delta 4}\hat{d}_{\delta}\left(\mathbf{x}\right) \tag{3}$$

$$\gamma_{D,v}\left(\mathbf{x},\boldsymbol{\theta}_{D,v}\right)=\theta_{D,v1}\ln\left(\frac{PGA}{g}\right)+\theta_{D,v2}\ln\left(\frac{H_p}{H_c}\right)+\theta_{D,v3}K_{soil}+\theta_{D,v4}\hat{d}_v\left(\mathbf{x}\right) \tag{4}$$

$$\gamma_{D,b}\left(\mathbf{x},\boldsymbol{\theta}_{D,b}\right)=\theta_{D,b1}\ln\left(\frac{PGA}{g}\right)+\theta_{D,b2}\hat{d}_v\left(\mathbf{x}\right) \tag{5}$$

These equations show that PGA has effects on predicting all three structural response quantities.

Tables 5-7 provide the mean values and the standard deviation of $\theta_{D,ki}$ and $\sigma_{D,k}$ together with their correlation coefficients. As shown in Table 5, the mean estimates of $\theta_{D,\delta 1}$ and $\theta_{D,\delta 2}$ are

Table 5 Posterior statistics of parameters in the column deformation model

$\boldsymbol{\Theta}_{D,\delta}$	Mean	Standarddeviation	Correlation coefficient			
			$\theta_{D,\delta 1}$	$\theta_{D,\delta 2}$	$\theta_{D,\delta 3}$	$\theta_{D,\delta 4}$
$\theta_{D,\delta 1}$	0.275	0.024				
$\theta_{D,\delta 2}$	0.929	0.059	0.23			
$\theta_{D,\delta 3}$	–1.445	0.089	–0.32	–0.86		
$\theta_{D,\delta 4}$	–0.465	0.022	–0.48	–0.70	0.95	
$\sigma_{D,\delta}$	0.475	0.020	0.02	–0.02	0.03	–0.01

Table 6 Posterior statistics of parameters in the column shear model

$\boldsymbol{\Theta}_{D,v}$	Mean	Standarddeviation	Correlation coefficient			
			$\theta_{D,v1}$	$\theta_{D,v2}$	$\theta_{D,v3}$	$\theta_{D,v4}$
$\theta_{D,v1}$	0.240	0.018				
$\theta_{D,v2}$	–0.439	0.056	–0.24			
$\theta_{D,v3}$	–0.177	0.032	–0.03	0.11		
$\theta_{D,v4}$	–0.355	0.015	–0.56	0.81	0.39	
$\sigma_{D,v}$	0.356	0.013	0.02	0.02	0.03	–0.04

Table 7 Posterior statistics of parameters in the bearing deformation model

$\boldsymbol{\Theta}_{D,b}$	Mean	Standard deviation	Correlation coefficient	
			$\theta_{D,b1}$	$\theta_{D,b2}$
$\theta_{D,b1}$	0.106	0.024		
$\theta_{D,b2}$	–0.168	0.010	–0.74	
$\sigma_{D,b}$	0.484	0.021	0.02	–0.1

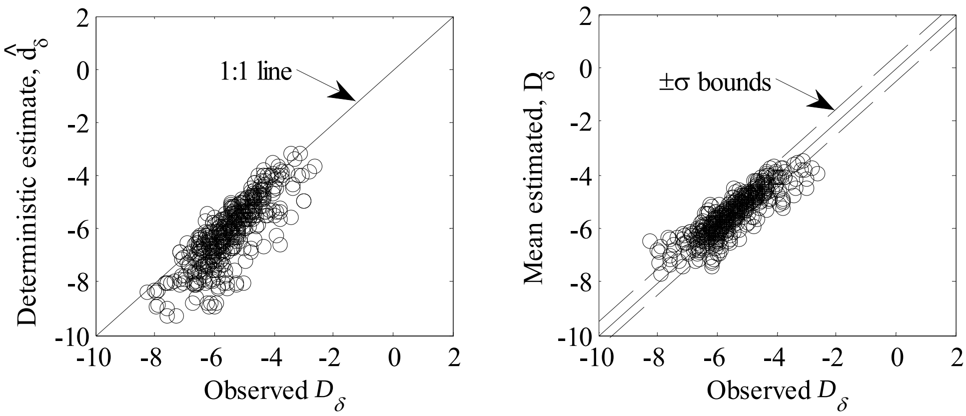

(a) Column deformation

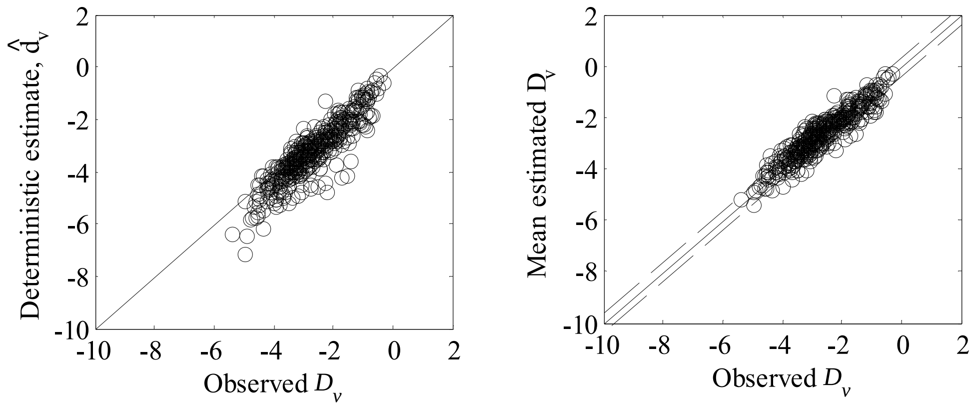

(b) Column shear

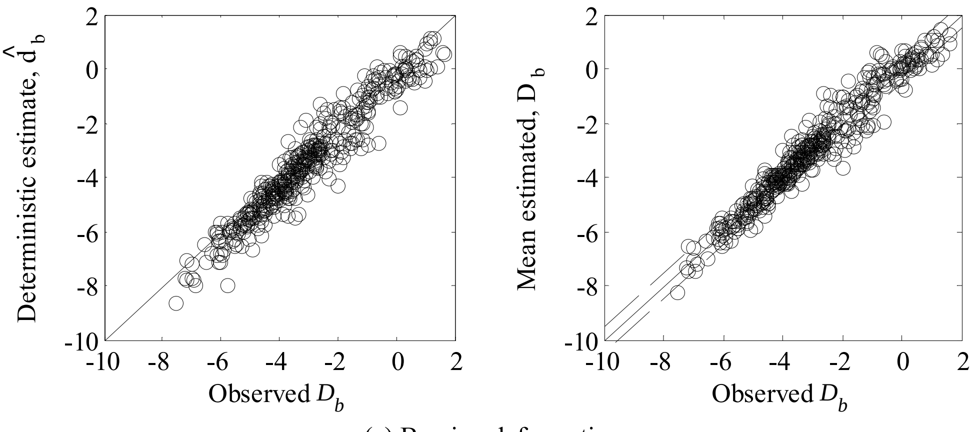

(c) Bearing deformation

Fig. 7 Developed probabilistic models in comparison with the corresponding deterministic models

positive, and those of $\theta_{D,\delta 3}$ and $\theta_{D,\delta 4}$ are negative. Referring to Eq. (2) and, this suggests that the deterministic model for predicting the column deformation underestimates or does not account for the effects of PGA and K_{ar} and overestimates the effects of S_{ba}. The quantity PGA has often been used to represent the severity of an earthquake ground motion (Karim and Yamazaki 2001, Shinozuka *et al.* 2001); however, PGA is absent in the deterministic model. The term $=\theta_{D,\delta 1}\ln(PGA/g)$ brings PGA back into the model. The underestimation of the rotational stiffness, K_{ar}, and the overestimation of the shape factor, S_{ba}, of the abutment bearings could be due to the fact that the pushover curve was developed using horizontal increasing forces while the bridge was seismically excited in three directions. The negative value of $\theta_{D,\delta 4}$ indicates a conservative bias in predicting $\hat{d}_{\delta}(\mathbf{x})$ as consistently shown in Fig. 7. With similar observations for Tables 6 and 7, PGA has an effect on the column shear and bearing deformation that is not accounted for in the deterministic models. Therefore, in addition to PSA, which is used in the deterministic demand models $\hat{d}_k(\mathbf{x})$, PGA is also informative in predicting the demands of interest. The negative value of $\theta_{D,v2}$ and $\theta_{D,v3}$ in Table 6 implies that the deterministic models tend to overestimate the effect of the depth of the drilled-shaft pile, H_p, and the flexibility of the soil around this pile, K_{soil}. This indicates that the interaction between the soil

Table 8 Posterior statistics of parameters in the trivariate model

$\mathbf{\Theta}_D$	Mean	Standard deviation	Correlation coefficient							
			$\theta_{D,\delta 1}$	$\theta_{D,\delta 2}$	$\theta_{D,\delta 3}$	$\theta_{D,\delta 4}$	$\theta_{D,v1}$	$\theta_{D,v2}$	$\theta_{D,v3}$	$\theta_{D,v4}$
$\theta_{D,\delta 1}$	0.269	0.023								
$\theta_{D,\delta 2}$	0.853	0.052	0.21							
$\theta_{D,\delta 3}$	–1.336	0.079	–0.29	–0.86						
$\theta_{D,\delta 4}$	–0.441	0.019	–0.46	–0.70	0.94					
$\theta_{D,v1}$	0.228	0.018	0.39	0.01	–0.00	–0.08				
$\theta_{D,v2}$	–0.318	0.042	–0.02	–0.06	0.09	0.09	–0.18			
$\theta_{D,v3}$	–0.090	0.024	0.03	–0.01	0.01	–0.00	–0.03	0.11		
$\theta_{D,v4}$	–0.315	0.012	–0.17	–0.04	0.06	0.11	–0.59	0.74	0.35	
$\theta_{D,b1}$	0.105	0.024	0.37	–0.02	0.03	–0.05	0.61	0.00	0.00	–0.28
$\theta_{D,b2}$	–0.168	0.010	–0.25	0.01	–0.02	0.08	–0.45	–0.02	–0.01	0.38
$\sigma_{D,\delta}$	0.476	0.020	0.01	–0.04	0.05	–0.00	0.01	0.01	0.01	–0.04
$\sigma_{D,v}$	0.360	0.014	0.00	–0.03	0.03	–0.01	0.02	0.04	0.05	–0.07
$\sigma_{D,b}$	0.484	0.021	0.01	–0.00	0.01	0.00	0.02	0.01	0.01	–0.04
$\rho_{D,\delta v}$	0.441	0.048	0.01	0.01	–0.01	–0.02	0.01	0.02	0.02	–0.06
$\rho_{D,\delta b}$	0.402	0.044	0.02	0.03	–0.02	–0.01	0.01	0.01	0.02	–0.02
$\rho_{D,vb}$	0.633	0.044	0.01	–0.00	0.01	0.01	–0.01	–0.03	–0.02	0.06

Table 8 Continued

	Correlation coefficient						
	$\theta_{D,b1}$	$\theta_{D,b2}$	$\sigma_{D,\delta}$	$\sigma_{D,v}$	$\sigma_{D,b}$	$\rho_{D,\delta v}$	$\rho_{D,\delta b}$
$\theta_{D,b2}$	–0.73						
$\sigma_{D,\delta}$	0.01	–0.03					
$\sigma_{D,v}$	0.01	–0.01	0.33				
$\sigma_{D,b}$	0.02	–0.09	0.19	0.49			
$\rho_{D,\delta v}$	0.02	–0.11	0.15	0.41	0.29		
$\rho_{D,\delta b}$	0.02	–0.08	0.13	0.21	0.32	0.49	
$\rho_{D,vb}$	0.01	–0.09	0.02	0.07	0.25	0.14	0.47

and the drilled shaft are not properly captured in the deterministic model. Similarly, $\theta_{D,v4}$ and $\theta_{D,b2}$ are negative suggesting that the deterministic models typically result in conservative estimates. However, there are difficulties in the interpretation of the numerical values of empirical regression coefficients in the case of high correlation between the parameters.

The probabilistic demand model for the column shear has the smallest standard deviation of the model error, $\sigma_{D,v} = 0.356$, and the demand models for column and bearing deformations have marginally higher standard deviations of the models errors, $\sigma_{D,\delta} = 0.475$ and $\sigma_{D,b} = 0.484$. Because the demands of deformation and shear on the column and the bearing are not independent under a seismic event, $\theta_{D,ki}$ and $\sigma_{D,k}$ are correlated. Gardoni *et al.* (2003) provided procedures to determine the statistics of these parameters and their correlation. Table 8 shows the posterior statistics of these parameters and the correlation coefficients, $\rho_{D,\delta v}$, $\rho_{D,\delta b}$ and $\rho_{D,vb}$, between the model errors. The estimates of the parameters are nearly the same as those in the univariate models when individual demands are considered separately as shown in Tables 5-7. As a result, the values of R^2 and R^2_{adj} for the trivariate models are also the same.

Fig. 7 compares the accuracy of the developed probabilistic demand models. The validity of the proposed models including the assumption of constant variance and normality of the model errors is confirmed by diagnostic plots (Rao and Toutenburg 1997). Values that are obtained using the deterministic model are plotted versus the observed values for the three structural response quantities on the left. Corresponding mean estimates using the newly developed demand models are plotted versus the observed values on the right. The solid 1:1 lines are where the predicted demands coincide with the observed demands. Two dashed lines above and below the 1:1 line represent the standard deviation of model errors. Fig. 7 shows that the deterministic models generally underestimate the responses as most data points are below the 1:1 lines. In addition, the deterministic models have significant uncertainties (shown by the scatter of the data), especially in predicting the column deformation and shear. The corresponding probabilistic demand models are successful in correcting the bias and reducing the uncertainties.

4. Probabilistic capacity models

The event that the column deformation, shear force, or the bearing deformation exceeds their limitsis considered as an undesired performance of the bridge system. The limits are defined as the capacities of structures. Probabilistic capacity models for the column deformation and shear force were developed by Gardoni *et al.* (2002) and denoted respectively as $C_\delta(\mathbf{x}, \mathbf{\Theta}_{C,\delta})$ and $C_v(\mathbf{x}, \mathbf{\Theta}_{C,v})$. Choe *et al.* (2007) later updated the parameters in these two models using the Bayesian updating approach and new laboratory test data for the column. Their models are used here with the developed probabilistic demand models to formulate a reliability analysis. The capacity model for quantity k is expressed as

$$C_k\left(\mathbf{x}, \boldsymbol{\theta}_{C,k}, \sigma_{C,k}\right) = \hat{c}_k\left(\mathbf{x}\right) + \gamma_{C,k}\left(\mathbf{x}, \boldsymbol{\theta}_{C,k}\right) + \sigma_{C,k}\varepsilon_{C,k} \tag{6}$$

where, similar to the demand model, $\hat{c}_k(\mathbf{x})$ is the capacity quantity k predicted using a deterministic model, $\gamma_{C,k}(\mathbf{x}, \boldsymbol{\theta}_{C,k})$ and $\sigma_{C,k}$ are the correction term and the standard deviation of the model error, respectively, and $\varepsilon_{C,k}$ is a standard normal variable.

Although an elastomeric bearing can sustain significantly large horizontal displacements, even exceeding the horizontal dimension of the bearing as tested in Chang and Seidensticker (1993), the bearing under such a large vertical load can easily buckle in the case of excessive horizontal displacement. The critical horizontal displacement beyond which the bearing looses stability is determined as discussed in Kelly and Naeim (1999). The natural logarithm of the critical deformation ratio or the deformation capacity, $\hat{c}_b(\mathbf{x})$, of a circular bearing is obtained as

$$\hat{c}_b\left(\mathbf{x}\right) = \ln\left(\frac{2R \cdot d_{crit}}{h_b}\right) \tag{7}$$

where, $d_{crit} = \cos\alpha_{crit}$. The bearing buckles when angle α, as defined in Fig. 4, reduces to α_{crit}. The value of α_{crit} can be obtained by solving the following equations

$$\frac{2}{\pi}\left(\alpha_{crit} - \sin\alpha_{crit}\cos\alpha_{crit}\right) = \left(\frac{P}{P_{crit}}\right)^2 \tag{8}$$

$$P_{crit} = \frac{\pi^2}{\sqrt{2}}\frac{R^3}{t_r}S_b \cdot G_b \tag{9}$$

where P is the vertical load and P_{crit} is the critical load. Parameters t_r, S_b or S_{bp}, and G_b are the thickness of elastomer or rubber, the shape factor, and the elastomer shear modulus of the bearing material.

A probabilistic capacity model should be used due to the presence of uncertainties associated with the assumptions made in developing this model. Based on the recommendations of Wen *et al.* (2004) regarding capacity uncertainty and modeling errors, the coefficient of variation for the deformation capacity is assumed to be equal to 30%. It is acknowledged that this assumption for the model error uncertainty can affect the fragility estimate of the bridge system. Future studies are needed to assess the uncertainty of the model error. Thus, the probabilistic capacity form of the bearing deformation can be given as

$$C_b(\mathbf{x}) = c_b(\mathbf{x}) + 0.3c_b(\mathbf{x})\varepsilon_{C,b} \tag{10}$$

5. Formulation of approximate fragility estimates

As discussed in Hirata *et al.* (1991) and Gardoni *et al.* (2002), the seismic fragility of a structure can be defined as the probability that the seismic demand on the structure is greater than or equal to its capacity given a determined set of ground motion parameters, $\mathbf{s}$. Thus, the seismic fragility of a structure regarding the response quantity k can be expressed as the conditional probability

$$F_k\left(\mathbf{s},\mathbf{\Theta}_k\right) = P\left[g_k\left(\mathbf{x},\mathbf{\Theta}_k\right) \le 0 \middle| \mathbf{s}\right] \tag{11}$$

where $\mathbf{\Theta}_k = (\mathbf{\Theta}_{C,k},\mathbf{\Theta}_{D,k})$. The performance function or limit state function, $g_k(\mathbf{x},\mathbf{\Theta}_k)$, is defined as

$$g_k\left(\mathbf{x},\mathbf{\Theta}_k\right) = C_k\left(\mathbf{x},\mathbf{\Theta}_{C,k}\right) - D_k\left(\mathbf{x},\mathbf{\Theta}_{D,k}\right) \tag{12}$$

Following Gardoni *et al.* (2002), predictive fragility estimates can be computed considering the variability in $\mathbf{\Theta}$ as

$$\tilde{F}_k\left(\mathbf{s}\right) = \int F_k\left(\mathbf{s},\mathbf{\Theta}_k\right) f\left(\mathbf{\Theta}_k\right) d\mathbf{\Theta}_k \tag{13}$$

where $f\left(\mathbf{\Theta}_k\right)$ is the posterior probability density function (PDF) of $\mathbf{\Theta}_k$.

In case of q limit states of which any limit being exceeded leads to the undesired performance of the structure, the predictive seismic fragility of the structure can be expressed as

$$\tilde{F}_{sys}\left(\mathbf{s}\right) = \int P\left[\bigcup_{k=1}^{q} g_k\left(\mathbf{x},\mathbf{\Theta}_k\right) \le 0 \middle| \mathbf{s}\right] f\left(\mathbf{\Theta}\right) d\mathbf{\Theta} \tag{14}$$

where $\mathbf{\Theta} = (\mathbf{\Theta}_1,\ldots,\mathbf{\Theta}_q)$.

Importance analysis can be used to reduce the complexity of reliability analysis by evaluating the effects of the variable randomness on the estimated probabilities. A large number of random variables make the reliability analysis computationally intensive. Based on the results of the importance analysis, only the randomness of important variables can be retained for the reliability analysis. Considering the limit state function k, the importance measure for a vector of n_r random variables, $\mathbf{z} = (\mathbf{x}, \boldsymbol{\Theta}, \boldsymbol{\varepsilon})$, can be written as (Der Kiureghian and Ke 1985)

$$\boldsymbol{\gamma}_k^T = \frac{\boldsymbol{\alpha}_k^T \mathbf{J}_{\mathbf{u}^*,\mathbf{z}^*} \mathbf{D}'}{\left| \boldsymbol{\alpha}_k^T \mathbf{J}_{\mathbf{u}^*,\mathbf{z}^*} \mathbf{D}' \right|} \tag{15}$$

where, $\boldsymbol{\alpha}_k$ is a normalized vector of the negative gradient of g_k at the design point in the standard normal space, $\mathbf{J}_{\mathbf{u}^*,\mathbf{z}^*}$ is the Jacobian of the transformation of unit normal vector $\mathbf{u}$ with respect to $\mathbf{z}$, evaluated at the design point, $\mathbf{z}^*$, $\mathbf{D}'$ is the diagonal matrix of the standard deviations of the normal variables, $\mathbf{z}' = \mathbf{z}^* + \mathbf{J}_{\mathbf{u}^*,\mathbf{z}^*}(\mathbf{u} - \mathbf{u}^*)$,which accounts for the uncertainty in each random variable. Following the general reliability theory (Ditlevsen and Madsen 1996), the design point is defined as the point on the failure or boundary surface in the space of the random variables $\mathbf{z}$ that is closest to the origin. Fig. 8 presents the results of the importance analysis for the example bridge regarding the three limit states when $PGA = 0.2g$. The model errors in both capacity and demand models, $\varepsilon_{C,k}$ and $\varepsilon_{D,k}$, are the most important random variables, especially for high values of PSA .

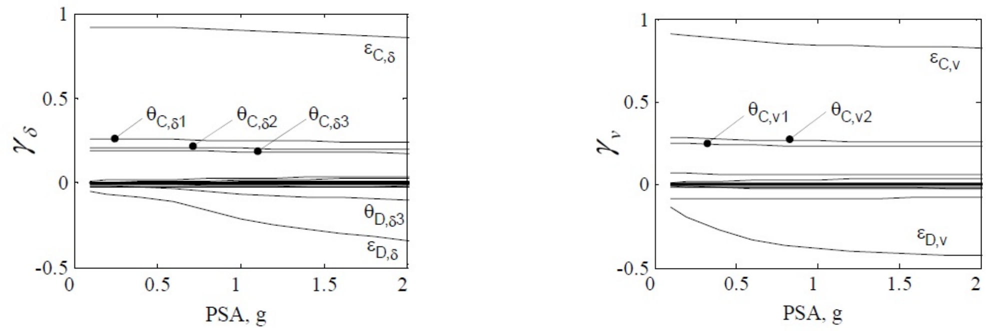

(a) Column deformation limit state (b) Column shear limit state

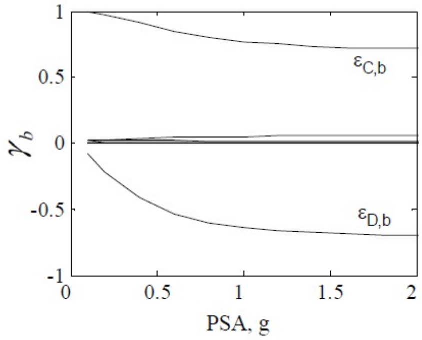

(c) Bearing deformation limit state

Fig. 8 Comparison of importance of random variables (*PGA*=0.2 g)

An approximate form of the fragility is developed based on this observation. The six model errors, $\varepsilon_{C,k}$ and $\varepsilon_{D,k}$, are kept random, while the other random variables are replaced with point estimates, (e.g. their mean values $\hat{\mathbf{x}}$ and $\hat{\mathbf{\Theta}}$). Because $\varepsilon_{C,k}$ and $\varepsilon_{D,k}$ are normally distributed random variables, the seismic fragility for limit state k can be determined following Choe *et al.* (2007) as

$$\hat{F}_k\left(\mathbf{s}\right)=F_k\left(\mathbf{s},\hat{\mathbf{\Theta}}_k\right)=1-\Phi\left(u_k\right) \tag{16}$$

where $\Phi(\cdot)$ is the cumulative distribution function (CDF) of a standard normal random variable and

$$u_k=\frac{\mu_{C_k}-\mu_{D_k}}{\sqrt{\sigma_{C_k}+\sigma_{D_k}^2}}=\frac{c_k(x)-\hat{d}_k(x)+\gamma_{C,k}(x,\theta_{C,k})-\gamma_{D,k}(x,\theta_{D,k})}{\sqrt{\sigma_{C,k}+\sigma_{D,k}^2}} \tag{17}$$

Following Zhong *et al.* (2008) and Huang *et al.* (2010), an approximate form for the system reliability in Eq. (14) can be written considering only the uncertainties in $\varepsilon_{C,k}$ and $\varepsilon_{D,k}$ as-

$$F_{sys}(\mathbf{s})=F_{sys}(\mathbf{s},\mathbf{\Theta})=P\left[\bigcup_{k=1}^{q} g_k(\hat{\mathbf{x}},\mathbf{\Theta}_k)\le 0\middle|\mathbf{s}\right]=1-\Phi_q(\mathbf{u},\mathbf{R}) \tag{18}$$

where $\Phi_q(\cdot)$ is the q-variate standard normal CDF, $\mathbf{u}=(u_\delta,u_v,u_b)$, and $\hat{\mathbf{R}}=[\hat{\rho}_{kl}]$, where $\hat{\rho}_{kl}$ is a point estimate of the correlation between g_k and g_l. Assuming the capacities are statistically independent of the demands, derivation from g_k and g_l results in

$$\hat{\rho}_{kl}=\frac{\rho_{C,kl}\sigma_{C,k}\sigma_{C,l}+\rho_{D,kl}\sigma_{D,k}\sigma_{D,l}}{\sqrt{(\sigma_{C,k}^2+\sigma_{D,k}^2)(\sigma_{C,l}^2+\sigma_{D,l}^2)}} \tag{19}$$

where $\hat{\rho}_{C,kl}$ is a point estimate of the correlation between $C_k(\hat{\mathbf{x}},\hat{\mathbf{\Theta}}_{C,k})$ and $C_l(\hat{\mathbf{x}},\hat{\mathbf{\Theta}}_{C,l})$ and $\hat{\rho}_{D,kl}$ is a point estimate of the correlation between $D_k(\hat{\mathbf{x}},\hat{\mathbf{\Theta}}_{D,k})$ and $D_l(\hat{\mathbf{x}},\hat{\mathbf{\Theta}}_{D,l})$.

One can either evaluate $\Phi_q(\cdot)$ using numerical methods for a multi-fold integral or using an alternative approximate and usually simpler approach (Pandey 1998, Melchers 1999) as

$$\Phi_q\left(\mathbf{u},\hat{\mathbf{R}}\right)=\Phi\left(u_{q|q-1}\right)\cdots\Phi\left(u_{k|k-1}\right)\cdots\Phi\left(u_{2|1}\right)\Phi\left(u_1\right) \tag{20}$$

where $u_{k|k-1}$ is obtained using the following recursive procedure

$$u_{m|k}=\frac{u_{m|k-1}+\rho_{mk|k-1}A_{k|k-1}}{\sqrt{1-\rho_{mk|k-1}^2 B_{k|k-1}}}\quad,\ 1\le k<m\le q \tag{21}$$

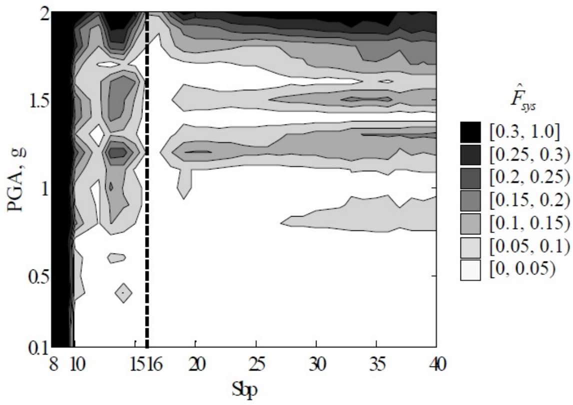

Fig. 9 Contours of the system fragility, $\hat{F}_{sys}$, as a function of ground motions (in terms of PGA) and the shape factor of the isolation bearing (S_{bp})

where $A_{k|k-1} = \phi(\rho_{k|k-1}) / \Phi(\rho_{k|k-1})$, $B_{k|k-1} = A_{k|k-1}(\rho_{k|k-1} + A_{k|k-1})$, $u_{1|0} = u_1$, and

$$\rho_{mk|(k-1)} = \frac{\rho_{mk|(k-2)} - \rho_{k(k-1)|(k-2)}\rho_{m(k-1)|(k-2)}B_{(k-1)|(k-2)}}{\sqrt{\left(1-\rho^2_{k(k-1)|(k-2)}B_{(k-1)|(k-2)}\right)\left(1-\rho^2_{m(k-1)|(k-2)}B_{(k-1)|(k-2)}\right)}} \tag{22}$$

where $\phi(\cdot)$ is the standard normal PDF, and $\rho_{mk|0} = \rho_{mk}$. For the application presented in this paper, $q = 3$, and k is δ, v, or b.

6. Reliability-based optimal design

The objective of the reliability-based optimal design can be to minimize the costs (e.g. construction or life-cycle cost) under reliability and structural constraints or to maximize the reliability of the structure under cost and structural constraints (Royset *et al.* 2001). In our study, the objective is to maximize the reliability or minimize the seismic fragility of an example bridge system with the optimal use of the isolation bearing. It is assumed that changing the bearing design has minimal effects on the total cost of a construction project. All the design variables given in Table 3 except the isolation bearing between the pier and the superstructure are structural constraints in the reliability-based optimal design problem. The shape factor of the elastomer layer of the bearing, S_{bp}, is a dimensionless quantity and has a wide range of variation as shown in Table 1. It is therefore the quantity of choice for the reliability-based optimal analysis.

Fig. 9 shows the fragility contours as a function of PGA and S_{bp}. The values of PGA used to construct the contour lines are those of the ground motions considered in the experimental design. For each ground motion, the value of PSA, which is needed in Eq. (1), is computed using the

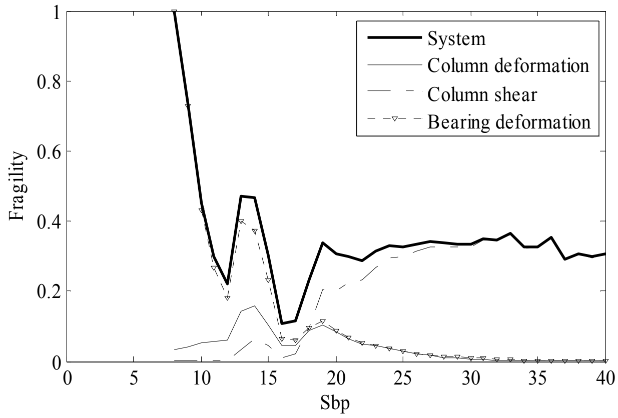

Fig. 10 Fragility versus the shape factor of the isolation bearing, S_{bp}, at PGA = 2.0 g

Newmark's Average Acceleration Method (Chopra 2000) based on the damping ratio of 5% and the natural period of the structural systems. Note that because the selected ground motions have different frequency contents, the computed values of PSA do not increase monotonically with PGA.

The fragility values increase with increasing darkness of the shading and are distinguished into four regions $0 \le \hat{F}_{sys} < 0.1$, $0.1 \le \hat{F}_{sys} < 0.2$, $0.2 \le \hat{F}_{sys} < 0.3$, $0.3 \le \hat{F}_{sys} \le 1.0$. For $S_{bp} \le 8$ the bearing fails due to the loss of stability; therefore, the system fragility is always 1.0 for this range of the shape factor. The dashed line at $S_{bp} = 16$ indicates the optimal value of S_{bp} that has the least value of fragility for any value of PGA. The natural period of the base-isolated bridge corresponding to $S_{bp} = 16$ is 1.424 s. For better understanding of the fragility distribution, Fig. 10 shows the fragility as a function of the shape factor at $PGA = 2.0g$. The fragility of the bridge system is compared with the fragilities in terms of the column deformation, the column shear, and the bearing deformation. The fragility of the bearing tends to decrease with S_{bp} while the fragility in terms of the shear increases. The fragility with regard to the column deformation increases first and decreases with the bearing deformation fragility for $S_{bp} > 19.0$. The optimal value for the shape factor is 16.0 as shown in Fig. 9.

7. Fragility estimates for an example bridge

Full fragility analysis is now carried out for the example isolated bridge with the optimal value of 16.0 for S_{bp}. Fig. 11compares the contours of the component fragility estimates versus PSA and PGA computed using the First-order Reliability Method (FORM) (Ditlevsen and Madsen 1996) (dashed lines) with all the 38 random variables, and the proposed approximate form as in Eq. (16), which uses only 2 random variables per mode of failure (solid lines). Each contour line

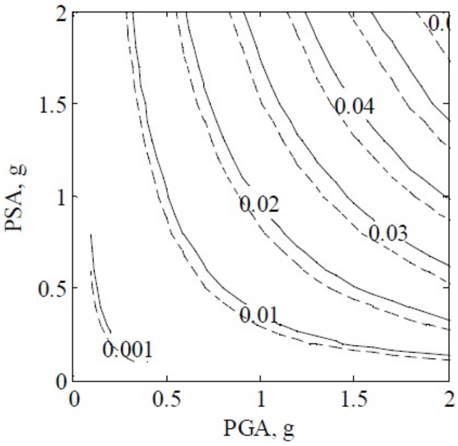

(a) Column deformation limit state

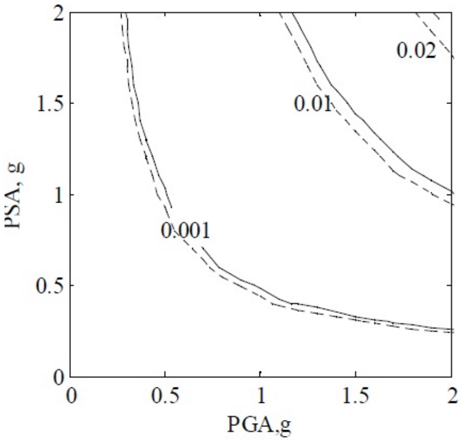

(b) Column shear limit state

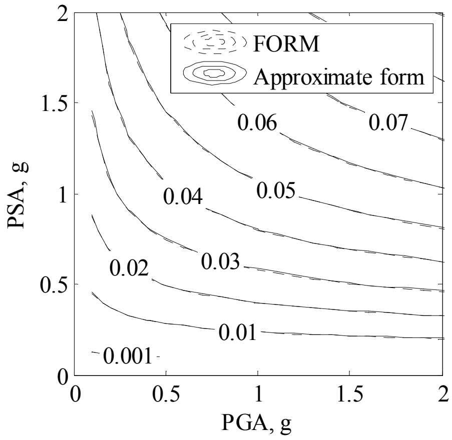

(c) Bearing deformation limit state

Fig. 11 Contour plots of the fragility estimates versus PSA and PGA computed usingthe proposed approximate form (solid lines) and FORM analysis (dashed lines)

connects pairs of points at the same level of fragility. Consistently with results of the importance analysis, the difference between the proposed approximate form and FORM analysis is small. The randomness or uncertainty included in the other variables can be neglected without losing significant accuracy. Fig. 11 shows that, for given PSA and PGA, failure is most likely to occur in the bearing. On the other hand, the column is well protected by the base isolation and the probabilities of failure of the column in deformation or shear are small relative to the probability of failure of the bearing.

Fig. 12 compares the system fragility obtained using the proposed approximate form as in Eq. (18) (solid lines) with that using an importance sampling technique (Hastings 1970) (dashed lines). As a termination criterion, we used 0.05 for the coefficient of variation of the failure probability estimate. The two approaches produce similar results. The system fragility in this figure is consistently higher than (or at least equal to) the highest component fragility in Fig. 11, confirming

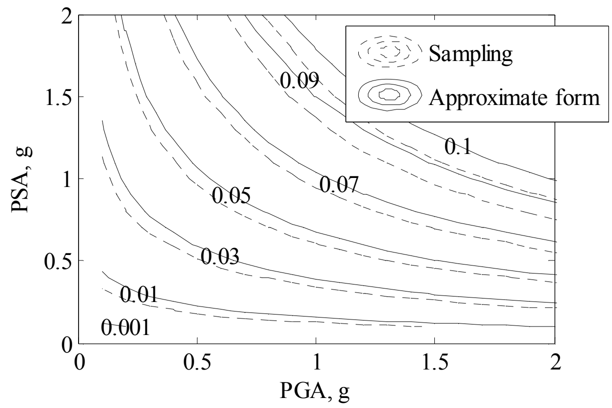

Fig. 12 Contour plot of the system fragility estimates versus PSA and PGA

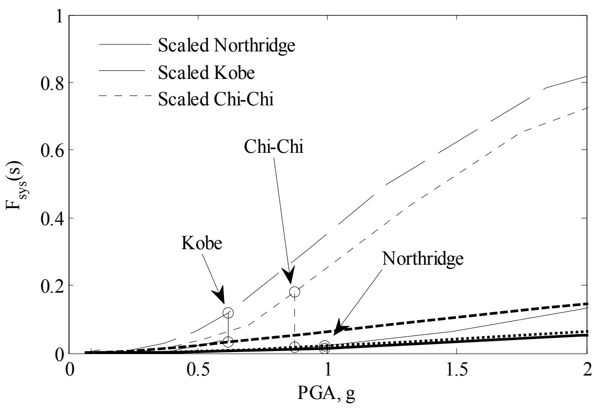

Fig. 13 Fragility of an isolated (thick lines) and non-isolated (thin lines) bridge under three example earthquakes

the system fragility is the union of the component fragilities.

Fig. 13 compares the point estimates of the system fragilities of the base-isolated bridge system with those of the corresponding non-isolated bridge system obtained by Huang *et al.* (2010) for the Northridge (SN #341), Kobe (SN #940) and Chi-Chi (SN #681) Earthquakes. The ground motions obtained from these events are scaled to create different sets of ground motion records. Each record provides one pair of PSA and PGA for a fragility estimate. The values of PSA are computed using the Newmark's Average Acceleration Method (Chopra 2000) based on the damping ratio of 5% and the natural period of the structural systems. The natural period of the non-isolated bridge is 0.966 s and that of the base-isolated bridge is 1.424 s as mentioned earlier.

Fig. 13 shows that the fragility estimates of the isolated bridge are significantly lower than that of the non-isolated bridge, especially for the ground motion associated to the Chi-Chi Earthquake. As shown in Fig. 3(a), the ground motion associated to the Chi-Chi Earthquake has its peak PSA close to the natural period of the non-isolated bridge ($T_n = 0.966$ s) and therefore the fragility experiences the biggest reduction due to the elongation of the natural period brought by the base isolation ($T_n = 1.424$ s). Fig. 13 also shows that the probability of failure for the ground motion associated to the Northridge Earthquake is less for both the non-isolated and isolated bridge than for the ground motions associated to the Chi-Chi and Kobe Earthquakes. Furthermore, elongating the natural period only has a limited benefit to the fragility estimates. This is because the values of PSA at the corresponding natural periods are relatively close.

8. Conclusions

Novel probabilistic demand models are developed to assess the seismic deformation and shear demands on RC columns and the deformation demand in bearings of base isolated RC bridges. The proposed models are unbiased and properly account for the underlying uncertainties. A general formulation is developed to assess the reliability of base isolated bridges using the proposed demand models. As an illustration, fragility analysis of an example bridge is carried out considering shear and deformation modes of failure for the bridge column and deformation mode of failure for the rubber-laminated bearings. While only three modes of failure are considered in the illustration, the reliability formulation is general and allows considering additional modes of failure. Their consideration would possible increase the estimated probabilities of failure. The paper quantifies the effectiveness of isolation bearings in reducing the vulnerability bridge systems by shifting the natural period of the systems into the less damaging range of the earthquake spectral acceleration. A reliability-based optimal design is conducted to find the value of the shape factor of the isolation bearing that minimizes the vulnerability of the example base-isolated bridge. An approximate formulation to estimate the fragility of base isolated RC bridges is also developed. The approximate formulation does not require specialized reliability computer programs and can more easily implemented in practice. It is noted that the model for the bearing is a standard simple model, typically used for small displacements. Further works is necessary to develop a more accurate model for large displacements.

Acknowledgments

The authors wish to acknowledge the assistance of Mr. Thanh Ngo.

References

AASHTO (the American Association of State Highway and Transportation Officials). (2007), *LRFD Bridge design specifications*, 4th Ed., Washington, D.C.

Abrahamson, N.A. and Silva, W.J (1997), "Empirical response spectral attenuation relations for shallow crustal earthquakes", *Seismol. Res. Lett.*, **68**(1), 94-127.

Albert, J. (2007), *Bayesian computation with R*, Springer, New York, N.Y.

Ang, A.H.S. and Tang, W.H. (2007), *Probability concepts in engineering-emphasis on applications in civil & environmental engineering*, 2nd Ed., Wiley, New York, N.Y.

API (the American Petroleum Institute). (1993), *Recommended practice for planning, designing, and constructing fixed offshore platforms – Load and resistance factor design*, Report RP2A-LRFD, American Petroleum Institute, Washington D.C.

ATC (the Applied Technology Council). (1996), *Seismic evaluation and retrofit of concrete buildings*, Report ATC-40, Redwood City, C.A.

ATC (the Applied Technology Council). (2005), *Improvement of nonlinear static seismic analysis procedures*, Report FEMA-440, Redwood City, CA.

Barker, R.M. and Puckett, J.A. (2007), *Design of highway bridges: An LRFD approach*, John Wiley and Sons, N.Y.

Bates, R.A., Buck, R.J., Riccomagno, E. and Wynn, H.P. (1996), "Experimental design and observation for large systems", *J. Royal Statist. Soc.*, **58**(1), 77-94.

Bommer, J.J. and Acevedo, A.B. (2004), "The use of real earthquake accelerograms as input to dynamic analysis", *J. Earthq. Eng.*, **8**(1), 43-91.

Box, G.E.P. and Tiao, G.C. (1992), *Bayesian inference in statistical analysis*, Wiley, New York, N.Y.

Caltrans. (1999), *Seismic design criteria*, California Dept. of Transportation, Sacramento, C.A.

Chang, Y.W. and Seidensticker, R.W. (1993), *Dynamic characteristics of bridge stone low shear modulus-high damping seismic isolation bearings*, Report ANL/RE-93/7, Reactor Engineering Division, Argonne National Laboratory, Argonne, I.L.

Cheng, F.Y., Jiang, H. and Lou, K. (2008), *Smart structures: Innovative systems for seismic response control*, Taylor & Francis Group, F.L.

Choe, D., Gardoni, P. and Rosowsky, D. (2007), "Closed-form fragility estimates parameter sensitivity and bayesian updating for RC columns", *J. Eng. Mech.-ASCE*, **133**(7), 833-843.

Chopra, A.K. (2000), *Dynamics of structures: Theory and applications to earthquake engineering*, Prentice Hall, Upper Saddle River, N.J.

Chopra, A.K. and Goel, R.K. (1999), *Capacity-demand-diagram methods for estimating seismic deformation of inelastic structures: SDF systems*, Report 1999/02, Pacific Earthquake Engineering Research Center, Univ. of California, Berkeley, C.A.

Der Kiureghian, A. and Ke, J.B. (1985), "Finite-element based reliability analysis of frame structures", *Proc., ICOSSAR '85, 4th Int. Conf. on Structural Safety and Reliability*, IASSAR, New York, 1, 395-404.

Ditlevsen, O. and Madsen, H.O. (1996), *Structural reliability methods*, Wiley, New York.

Fajfar, P. (1999), "Capacity spectrum method based on inelastic demand spectra", *Earthq. Eng. Struct. D.*, **28**(9), 979-993.

FEMA (the Federal Emergency Management Agency). (1997), *NEHRP Commentary on the guidelines for the seismic rehabilitation of buildings*, Report FEMA-274, the Federal Emergency Management Agency, Washington, D.C.

Freeman, S.A. (1998), "The capacity spectrum method as a tool for seismic design", *Proceedings of the Eleventh European Conference on Earthquake Engineering*, Paris, France, 6-11.

Gardoni, P., Der Kiureghian, A. and Mosalam, K.M. (2002), "Probabilistic capacity models and fragility estimates for RC columns based on experimental observations", *J. Eng. Mech.-ASCE*, **128**(10), 1024-1038.

Gardoni, P., Mosalam, K.M. and Der Kiureghian, A. (2003), "Probabilistic seismic demand models and fragility estimates for RC bridges", *J. Earthq. Eng.*, **7**(1), 79-106.

Hasting, W.K. (1970), "Monte Carlo sampling methods using markov chains and their applications", *Biometrika*, **57**(1), 97-109.

Hirata, K., Kobayashi, Y., Kameda, H. and Shiojiri, H. (1991), "Fragility of seismically isolated FBR structure", *Nucl. Eng. Des.*, **128**(1991), 227-236.

Huang, Q., Gardoni, P. and Hurlebaus, S. (2010), "Probabilistic seismic demand models and fragility estimates for reinforced concrete highway bridges with one single-column bent", *J. Eng. Mech.-ASCE*, **136**(11), 1340-1353.

Karim, K.R. and Yamazaki, F. (2001), "Effect of earthquake ground motions on fragility curves of highway bridge piers based on numerical simulation", *Earthq. Eng. Struct. D.*, **30**(12), 1839-1856.

Karim, K.R. and Yamazaki, F. (2003), "A simplified method of constructing fragility curves for highway bridges", *Earthq. Eng. Struct. D.*, **32**(10), 1603-1626.

Karim, K.R. and Yamazaki, F. (2007), "Effect of isolation on fragility curves of highway bridges based on simplified approach", *Soil Dyn. Earthq. Eng*., **27**(5), 414-426.

Kelly, J.M. and Naeim, F. (1999), *Design of seismic isolated structures*, John Wiley & Sons, N.Y.

Luco, N. (2002), *Probabilistic seismic demand analysis, SMRF connection fractures, and near-source effects*, Ph.D. Dissertation, Dept. of Civil and Environmental Engineering, Stanford University, California.

Mackie, K. and Stojadinovic, B. (2003), *Seismic demands for performance-based design of bridges*, Report 2003/16, Pacific Earthquake Engineering Research Center, University of California, Berkeley, C.A.

McKenna, F., Fenves, G.L. and Scott, M.H. (2003), *Open system for earthquake engineering simulation* <http://opensees.berkeley.edu/>, Pacific Earthquake Engineering Research Center, Univ. of California, Berkeley, C.A.

Melchers, R.E. (1999), *Structural reliability analysis and prediction*, 2nd Ed., John Wiley and Sons, Chichester, England.

Pandey, M.D. (1998), "An effective approximation to evaluate multinormal integrals", *Struct. Saf*., **20**(1), 51-67.

PEER (The Pacific Earthquake Engineering Research Center). (2009), *PEER strong ground motion database*, <http://peer.berkeley.edu> (Jan. 4, 2009).

Priestley, M.J.N., Seible F. and Calvi, G.M. (1996), *Seismic design and retrofit of bridges*, John Wiley and Sons, N.Y.

Qiang, H., Xiuli, d., Jingbo, L., Zhongxian, L., Liyun, L. and Jianfeng, Z. (2009), "Seismic damage of highway bridges during 2008 Wenchuan earthquake", *Earthq. Eng. Eng. Vib*., **8**(2), 263-273.

Rao, C.R. and Toutenburg, H. (1997), *Linear models, least squares and alternatives*, Springer, New York.

Rossi, P.E., Allenby, G.M. and McCulloch, R. (2005), *Bayesian statistics and marketing*, John Wiley and Sons, N.Y.

Royset, J.O., Der Kiureghian, A. and Polak, E. (2001), "Reliability-based optimal design of series structural systems", *J. Eng. Mech*., **127**(6), 607-614.

Ryan, K.L., Kelly, J.M. and Chopra, A.K. (2005), "Nonlinear model for lead-rubber bearings including axial-load effects", *J. Eng. Mech.-ASCE*, **131**(12), 1270-1278.

Sacks, J., Welch, W.J., Mitchell, T.J. and Wynn, H.P. (1989), "Design and analysis of computer experiments", *Statistic. Sci*., **4**(4), 409-423.

Sheather, S.J. (2008), *A modern approach to regression with R*, Springer, New York, N.Y.

Shinozuka, M., Feng, M.Q., Kim, H., Uzawa, T. and Ueda, T. (2001), *Statistical analysis of fragility curves*, Report MCEER2001, Department of Civil and Environmental Engineering, University of Southern California, Los Angeles, C.A.

Shome, N. and Cornell, C.A. (1999), *Probabilistic seismic demand analysis of nonlinear structures*, Report RMS-35, Department of Civil Engineering, Stanford Univ., Stanford, C.A.

Watson-Lamprey, J. and Abrahamson, N. (2006), "Selection of ground motion time series and limits on scaling", *Soil Dyn. Earthq. Eng*., **26**, 477-482.

Weisberg, S. (2005), *Applied linear regression*, 3rd Ed., John Wiley and Sons, Hoboken, N.J.

Wen, Y.K., Ellingwood, B.R. and Bracci, J.M. (2004), *Vulnerability function framework for con-sequence-based engineering*, Report DS-4, Mid-America Earthquake Center, Univ. of Illinois, Urbana-Champaign, I.L.

Wilde, K., Gardoni, P. and Fujino, Y. (2000), "Base isolation system with shape memory alloy device for elevated highway bridges", *Eng. Struct*., **22**(3), 222-229.

Zhong, J., Gardoni, P., Rosowsky, D. and Haukaas, T. (2008), "Probabilistic seismic demand models and fragility estimates for reinforced concrete bridges with two-column bents", *J. Eng. Mech.-ASCE*, **134**(6), 495-504.

JL